

Geophysical Research Letters

RESEARCH LETTER

10.1029/2019GL084818

Key Points:

- A multiproxy geochemical study supports claims that both a comet impact and volcanism occurred at the Paleocene-Eocene boundary
- The comet is estimated to be small with ~0.4 Gt carbon
- Climate modeling indicates that the comet impact might have caused transient cooling and reduction in precipitation

Supporting Information:

- Supporting Information S1

Correspondence to:

Z. Liu,
geozy.liu@outlook.com

Citation:

Liu, Z., Horton, D. E., Tabor, C., Sageman, B. B., Percival, L. M. E., Gill, B. C., & Selby, D. (2019). Assessing the contributions of comet impact and volcanism toward the climate perturbations of the Paleocene-Eocene Thermal Maximum. *Geophysical Research Letters*, 46, 14,798–14,806. <https://doi.org/10.1029/2019GL084818>

Received 1 AUG 2019

Accepted 17 DEC 2019

Accepted article online 19 DEC 2019

Published online 27 DEC 2019

Assessing the Contributions of Comet Impact and Volcanism Toward the Climate Perturbations of the Paleocene-Eocene Thermal Maximum

Zeyang Liu¹ , Daniel E. Horton² , Clay Tabor³ , Bradley B. Sageman² , Lawrence M.E. Percival^{4,5}, Benjamin C. Gill⁶ , and David Selby^{1,7}

¹Department of Earth Sciences, Durham University, Durham, UK, ²Department of Earth and Planetary Sciences, Northwestern University, Evanston, IL, USA, ³Department of Geosciences, University of Connecticut, Storrs, CT, USA,

⁴Institut des sciences de la Terre, Géopolis, Université de Lausanne, Lausanne, Switzerland, ⁵Analytical, Environmental and Geochemistry Group, Vrije Universiteit Brussel, Brussels, Belgium, ⁶Department of Geosciences, Virginia Polytechnic Institute and State University, Blacksburg, VA, USA, ⁷State Key Laboratory of Geological Processes and Mineral Resources, School of Earth Resources, China University of Geosciences, Wuhan, China

Abstract The Paleocene-Eocene Thermal Maximum is marked by a prominent negative carbon-isotope excursion, reflecting the injection of thousands of gigatons of isotopically light carbon into the atmosphere. The sources of the isotopically light carbon remain poorly constrained. Utilizing a multiproxy geochemical analysis (osmium isotopes, mercury, sulfur, and platinum group elements) of two Paleocene-Eocene boundary records, we present evidence that a comet impact and major volcanic activity likely contributed to the environmental perturbations during the Paleocene-Eocene interval. Additionally, Earth system model simulations indicate that stratospheric sulfate aerosols, commensurate with the impact magnitude, were likely to have caused transient cooling and reduced precipitation.

Plain Language Summary The Paleocene-Eocene Thermal Maximum (~55.9 Ma) records a period of climate warming associated with the injection of thousands of gigatons of carbon into the atmosphere. However, the sources of the carbon are still unclear. Our study uses geochemical data (osmium isotopes, mercury, sulfur, and platinum group elements) of two North Atlantic Ocean drill cores across the Paleocene-Eocene interval to suggest that both a comet impact and large-scale volcanism occurred at that time. The comet is estimated to be small (~3.3 km diameter) with ~0.4 Gt carbon and thus cannot be responsible for the Paleocene-Eocene Thermal Maximum. However, climate modeling suggests that the comet impact might have caused transient cooling and reduced precipitation.

1. Introduction

The Paleocene-Eocene Thermal Maximum (PETM; ~55.9 Ma) was characterized by the rapid release of several thousand gigatons ($\geq 3,000$ – $10,000$ Gt) of isotopically light carbon into the ocean and atmosphere, causing rapid global warming (Gingerich, 2003; Gutjahr et al., 2017; Schmitz & Pujalte, 2003; Wing et al., 2005; Wright & Schaller, 2013; Zachos et al., 2001; Zeebe et al., 2009). The main evidence for this carbon-cycle perturbation is a negative excursion in the carbon-isotope composition of both organic and inorganic matter (up to 6‰) in global PETM stratigraphic records (Bowen et al., 2015; Gutjahr et al., 2017; Wright & Schaller, 2013; Zachos et al., 2001; Zeebe et al., 2009). Commonly proposed sources of the carbon include volcanic gas emissions related to the emplacement of the North Atlantic Igneous Province [NAIP; Gutjahr et al., 2017; Saunders, 2016], metamorphism of organic-rich rocks by magmatic sills (Svensen et al., 2004), melting of methane hydrates and/or permafrost (DeConto et al., 2012; Dickens et al., 1995), and oxidization of marine sedimentary organic matter (Higgins & Schrag, 2006). An extraterrestrial impact has also been proposed as an alternative/additional contributor to the PETM, with iridium (Ir) enrichments identified within PETM strata in Western Slovenia (Dolenc et al., 2000) and Zumaya, Spain (Schmitz et al., 1997). Although these Ir anomalies have also been interpreted to be of volcanic origin (Schmitz et al., 2004), additional support for an extraterrestrial impact during the Paleocene-Eocene (P-E) transition was recently interpreted based on glass spherules (microtektites and microkrystites) and shocked-quartz reported from the base of the negative carbon-isotope excursion (CIE) in three stratigraphic records from the North Atlantic Ocean: Wilson Lake and Millville, New Jersey—both expanded continental shelf sites with organic-rich silty sediments (ODP

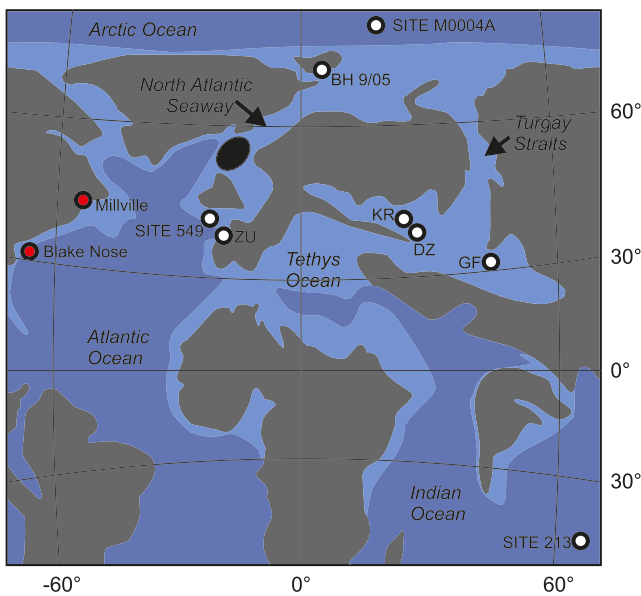


Figure 1. Map of sample locations. Red circles are for this study, and white circles are for previous studies (Dickson et al., 2015; Ravizza et al., 2001; Wieczorek et al., 2013). KR = Kheu River, Karbardino-Balkaria; DZ = Dzhengutay, Dagestan; GF = Guru-Fatima, Tajikistan; ZU = Zumaya, Spain; site numbers refer to Deep Sea Drilling Program (Sites 213 and 549) and Integrated Ocean Drilling Program (Site M0004A) cores. The black ellipse represents the zone of transient uplift associated with the North Atlantic Igneous Province mantle plume. Base map after Dickson et al. (2015).

the organic fraction of the samples and thus liberate hydrogenous Re and Os, avoiding the contamination from detrital Re and Os (Selby & Creaser, 2003). About 1 g sample powder with a known amount of a mixed tracer ($^{190}\text{Os} + ^{185}\text{Re}$) solution and 8 ml of 0.25 g/g $\text{Cr}^{\text{VI}}\text{-H}_2\text{SO}_4$ solution were digested in a sealed carius tube for 48 hr at 220 °C. Rhenium was isolated from the acid using $\text{NaOH}\text{-C}_3\text{H}_6\text{O}$ solvent extraction and anion chromatography. Osmium was purified using solvent extraction (CHCl_3) and microdistillation methods. The isolated Re and Os fractions were loaded onto Ni and Pt filaments, respectively (Selby et al., 2007). Isotopic measurements were determined using negative thermal ionization mass spectrometry (Creaser et al., 1991).

2.2. PGE Analysis

Powder samples were digested for PGE analysis using a modified method from Chu et al. (2015). The powdered shale (~1 g) plus a known amount of mixed Ir-Ru-Pt-Pd tracer solution and inverse aqua-regia (3 ml 11N HCl and 6 ml 16N HNO_3) were digested in sealed carius tubes at 220 °C for 72 hr. The Ir-Ru-Pt-Pd were then purified using an anion exchange column and Eichrom-LN column. The Pd and Ir-Pt-Ru fractions were measured by inductively coupled plasma mass spectrometry on a ThermoFinnigan Element 2 at Durham University. Mixed solutions of natural PGEs and solutions of Hf, Zr, Y, and Mo (all at 1 ng/g concentrations) were used to quantify the degree of mass fractionation and the production rates of HfO^+ , ZrO^+ , YO^+ , and MoO^+ (which possess oxides of equivalent mass to isotopes of Ir⁺, Pt⁺, and Pd⁺) before and after the analysis.

2.3. Hg Analysis

Mercury (Hg) concentrations were determined on a Mercury Analyzer RA 915 F coupled to a PYRO-915+ Pyrolyzer (Lumex) at the University of Lausanne (Switzerland), broadly following the method outlined in Percival et al. (2017). Mercury in the solid sample was volatilized by direct thermal evaporation and the resultant gas analyzed by atomic absorption spectrometry (Sholupov & Ganeyev, 1995). At least two measurements per sample, using 100 ± 2 mg powdered sample, were conducted to check reproducibility of

174AX: Schaller et al., 2016); and Blake Nos—a condensed sequence of carbonate-rich pelagic sediments (ODP Hole 1051B; Schaller et al., 2016; Schaller et al., 2019). The Blake Nose core documents the entire PETM CIE (Katz et al., 1999). In contrast, the Millville archive only captures the onset of the CIE as this record is truncated by an erosional surface about 12.5 m above the initial CIE (Wright & Schaller, 2013).

To further investigate the potential roles and temporal relationships of the proposed volcanism and impact events, we present new high-resolution osmium-isotope (Os_i) stratigraphy from the PETM interval of the Millville and Blake Nose cores (see Figure 1), coupled with mercury (Hg), pyrite sulfur (S), platinum group element (PGE; Pt-Pd-Ir-Ru), and total organic carbon (TOC) data. A geochemistry model estimates the impactor to have little amount of carbon (~0.4 Gt), thus cannot cause the PETM warming. We also present an Earth system model simulation to investigate the climate feedbacks resulting from any sulfur emissions associated with the postulated impact event.

2. Methods

Before crushing, all samples were polished to eliminate contamination from cutting and drilling marks. The samples were then air dried at 60 °C for ~12 hr and broken into chips with no metal contact. Samples were crushed to a fine powder (~30 μm) in a Zirconia ceramic dish using a shatterbox.

2.1. Re-Os Analysis

Re-Os isotope analysis was carried out at Durham University. For sample digestion, a $\text{Cr}^{\text{VI}}\text{-H}_2\text{SO}_4$ solution was employed to preferentially dissolve

the analysis, which was typically better than $\pm 10\%$. The measurements were calibrated using the Certified Reference Material NCS DC73309 (Chinese stream sediment), which has a Hg concentration of 72 ± 9 ppb. Four standards were measured at the start of an analytical run, with a further standard measured after each subsequent set of 10 unknown measurements to check for machine drift.

2.4. TOC Analysis

Powdered samples were analyzed for weight percent concentration of total carbon by combustion at 950°C in a stream of O₂. Total inorganic carbon (TIC) was analyzed by acidification using 10% phosphoric acid. Sample carbon converted to CO₂ by each preparation method is quantified by coulometric titration (Engleman et al., 1985; Huffman, 1977). TOC is calculated as the difference between wt% total carbon and TIC. The TIC value is converted to wt% calcium carbonate by stoichiometric calculation (wt% TIC \times 8.333), with the assumption that negligible quantities of inorganic carbon were present as minerals other than calcium carbonate.

2.5. Pyrite Sulfur Analysis

Pyrite sulfur was extracted from powdered samples using the chromium reduction of procedure of Canfield et al. (1986). Between 0.3 and 1 g of sample powder was reacted with ~40 ml of 1 M chromous chloride solution and heated for 2 hr in a specialized distillation line under nitrogen atmosphere. The sulfur liberated from the sample was precipitated as zinc sulfide and later converted to silver sulfide. This precipitate was dried and weighed to quantify to the pyrite sulfur content of the sample. Reproducibility was within 5% for all repeat extractions of a subset of the samples.

3. Results

At Millville, Hg concentrations are ~10 ppb below the P-E boundary, but double across that horizon to 20–25 ppb, and remain elevated up section. The Hg/TOC values show a similar trend to the Hg abundance, with an increase across the P-E boundary (40 to 60 ppb/wt. %) and elevated ratios maintained up section (~60 ppb/wt. %). At Blake Nose, the Hg concentration is about 2–4 ppb below the P-E boundary and increases slightly to ~7 ppb across that horizon. Two further Hg excursions to 30 and 20 ppb are also present above the P-E boundary at Blake Nose. TOC contents from the Blake Nose samples are generally too low (<0.2 wt%) to yield reliable Hg/TOC ratios [see Jones et al., 2019]. An elevation in Hg at the base of and within the main body of the PETM CIE is broadly consistent with previous investigations, although individual sedimentary records appear to show different patterns of these enrichments (Jones et al., 2019; Keller et al., 2018). Recent studies indicated that Hg enrichments could also be associated with increased sulfur/pyrite contents in highly reducing conditions (Shen et al., 2019). However, the Hg concentrations and Hg/TOC ratios exhibit no relationship with pyrite-S content at either site (Figures 2 and S1 and Tables S3 and S4).

Measured Re and Os abundances are significantly enriched in the more organic-rich sediments of Millville (Re: 5.3–11.4 ppb and Os: 92.1–321.9 ppt) compared to the calcareous pelagic sediments from Hole 1051B (Re: 0.04–0.23 ppb and Os: 26.8–146.2 ppt; Tables S1 and S2). Concentrations of the common Os isotope (¹⁹²Os), which represent the best estimate of hydrogenous Os complexed by organic matter at the time of deposition, become significantly enriched in the sedimentary units across the P-E boundary at both Millville and Blake Nose (Figure 2 and Tables S1 and S2), with above-background contents sustained well into the main body of PETM CIE. The ¹⁸⁷Os/¹⁸⁸Os values calculated at the time of deposition (Os_i) at the two sites range from 0.30 to 0.42 and are in good agreement with Os_i data from other P-E sections (Dickson et al., 2015; Wieczorek et al., 2013). At Millville, the Os_i values are relatively unradiogenic (0.33–0.38) below the P-E boundary, with a shift toward an even more unradiogenic composition (0.38 to 0.30) at the boundary itself. The Os_i then rapidly returns to the preexcursion values (0.38), followed by a gradual trend toward a more radiogenic composition upsection (0.38 to 0.42; Figure 2). At Blake Nose, the Os_i values are unradiogenic (0.36–0.37) below the P-E boundary, with a nominal decrease (0.36 to 0.35) across the P-E boundary, followed by a nominal increase to 0.36 and then a decrease to 0.35 (Figure 2). However, it should be noted that all variations in Os_i at Blake Nose are within analytical uncertainty.

No PGE anomaly is observed at the P-E boundary (Ir: 0.02–0.11 ppb, Ru: 0.10–3.04 ppb, Pd: 0.69–2.57 ppb, and Pt: 0.29–2.78 ppb; Figure S2 and Table S5), with the PGE values generally being lower than that reported

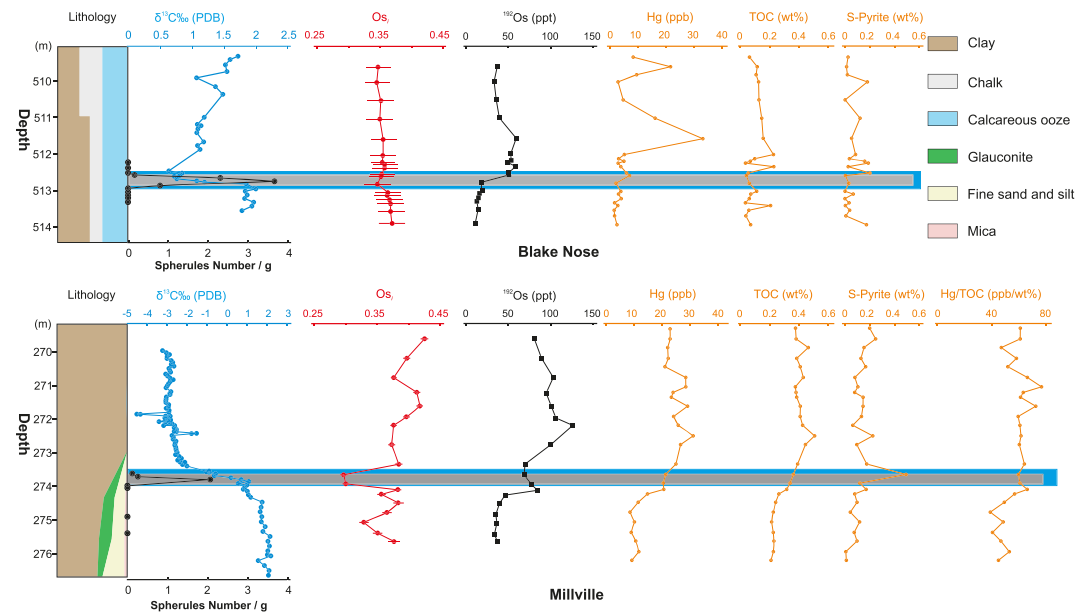


Figure 2. Summary of carbon-isotope, Os_i, ¹⁹²Os, Hg, TOC, pyrite sulfur, and Hg/TOC data. Carbon-isotope data for Blake Nose are from Katz et al. (1999). Carbon-isotope data for Millville site is from Wright and Schaller (2013). Spherule data are from Schaller et al. (2016). Blue zone marks the base of the negative carbon isotope excursion at the P-E boundary; gray zone marks the interval where spherules are present.

from the Cretaceous-Paleogene boundary (Goderis et al., 2013). Further, the Ir values are lower than that of the Zumaya (0.037–0.423 ppb) and Slovenia (0.1–2.3 ppb) sections.

4. Discussion and Implications

In the studied sections, Hg concentrations and Hg/TOC exhibit no relationship with pyrite sulfur content (Figure 2 and S1 and Tables S3 and S4), suggesting a lack of a local redox control on the Hg contents. The Hg enrichments at Millville do correlate with an increased clay content in the section (Figure 2), potentially highlighting a lithological role on the Hg content of these sediments. As such and given the sporadic nature of the Hg peaks at Blake Nose, it cannot be unambiguously stated that the Hg trends reported here reflect increased volcanism during the PETM. However, a trend of Hg enrichments in PETM strata has also been reported from several other locations and largely been interpreted as resulting from processes relating to volcanic/intrusive activity of the NAIP (Jones et al., 2019; Keller et al., 2018). Thus, while a sedimentological control on the Hg trends from Millville and Blake Nose cannot not be excluded, a NAIP-related volcanic/thermogenic source for these Hg enrichments would be consistent with the interpretations of previous PETM Hg studies. The difference in exact patterns of Hg enrichment in global PETM strata (Jones et al., 2019), as well as other events (Percival et al., 2018), has been attributed to one/both of local sedimentological processes specific to each paleoenvironmental setting or the distance of an archive from the proposed source (Jones et al., 2019; Percival et al., 2018). To date, there are no constraints on the potential delivery of Hg to the Earth's surface by an extraterrestrial impact body. However, if an influx of impact-derived Hg did occur and was preserved in the PETM geological record, then a single pulse of Hg enrichment would be expected. By contrast, the Hg and Hg/TOC exhibit consistently elevated (Millville) and repeated peaks (Blake Nose) at and above the P-E boundary (Figure 2), and no other PETM records show a single-pulse pattern of Hg enrichment that would be consistent with an impact-related influx.

The short-lived unradiogenic shift in Os_i at the P-E boundary (Figure S3; Dickson et al., 2015; Schmitz et al., 2004; Wieczorek et al., 2013; this study) could have been caused by an increase in unradiogenic Os input or reduced radiogenic input from decreased weathering (Peucker-Ehrenbrink & Ravizza, 2000). A reduction in weathering rates during a hyperthermal period seems unlikely as enhanced weathering of silicate rocks is considered a negative feedback mechanism to buffer the increase of atmospheric CO₂ (Walker et al.,

1981). Previously, a decrease in $^{187}\text{Os}/^{188}\text{Os}_i$ of ~ 0.05 has been found at the base of the PETM at Kheu River, Guru-Fatima, and Zumaya, Spain [Figure 1; Dickson et al., 2015; Schmitz et al., 2004]. A larger magnitude of unradiogenic Os-isotope excursion (~ 0.3) was found at Svalbard Core BH9/05 in the Central basin ~ 8 Kyr before the onset of the PETM (Wieczorek et al., 2013). All the Os_i excursions have been linked with volcanism related to the NAIP, with the larger unradiogenic Os-isotope shift at Svalbard being attributed to the proximity of that section to the NAIP (Figure 1; Dickson et al., 2015; Wieczorek et al., 2013). However, although the Os_i shift recorded at Svalbard correlates with an Hg and Hg/TOC enrichment, elevated Hg (Hg/TOC) values in that section are also observed below and continue considerably above that level, whereas Os_i returns to preshift values abruptly (Jones et al., 2019). Similarly, the Os_i unradiogenic shift of the Millville core is limited to the P-E boundary, whereas elevated Hg (Hg/TOC) values continue above the base of the PETM. The discrepancy between Hg and Os_i trends may have resulted from a sedimentological rather than volcanic control on the observed Hg enrichments or a combination of magmatic and thermogenic Hg emissions (Jones et al., 2019).

The coincidence of shifts to more unradiogenic Os_i values (although the shift at Blake Nose is within uncertainty) in the same stratigraphic intervals where silicate glass spherules (microtektites and microkrystites) and shocked quartz are reported (Millville and Blake Nose; Figure 2) opens the possibility of an extraterrestrial source as a potential alternative/additional contribution to the Os influx to the ocean. However, it remains unclear how much of the Os was derived from the impactor and how much from volcanism. To date, no significant extraterrestrial origin PGE anomalies have been found across the P-E boundary; the Ir anomaly associated with the CIE at Zumaya and the PGEs enrichments at the P-E boundary of Goriska Brda (Slovenia) are argued to be caused by volcanic activity or redox changes (Dolenec et al., 2000; Schmitz et al., 2004). Because there is no enrichment in the other PGEs (Pt, Pd, Ir, and Ru) within the spherule horizon, we hypothesize that the impactor was most likely to have been a volatile-rich comet that possessed lower PGEs contents compared to most other extraterrestrial bodies (Jansa, 1993). Other types of impactor are possible but would likely yield a different signature of PGEs and other elements (Wasson & Kallemeyn, 1988). This hypothesis is consistent with the vesicular volatile degassing structure of the shocked quartz (Schaller et al., 2016). As such, the small unradiogenic Os_i shift at the PETM could reflect osmium at least partially derived from a comet impact.

Assuming that the unradiogenic Os_i shift was partially/entirely caused by a comet, the impactor size can be estimated based on the sedimentary osmium isotope record and the oceanic Os inventory, as well as the impactor composition (Paquay et al., 2008). Estimating the size of the impactor at the PETM is difficult, given the uncertainty in the chemical composition of the comet, and that the Os_i excursion could be potentially driven by volcanism as well as/in addition to any impactor. The Millville record is used here as it features the highest resolution; thus, it may capture the most accurate unradiogenic Os_i shift. If we assume that the impact body is responsible for the full manifestation of the observed unradiogenic Os_i shift (~ 0.08 at Millville), the estimated maximum diameter of the impactor is ~ 3.3 km (see supporting information S1). However, it cannot be ruled out that the impactor was smaller if part of the Os_i shift resulted from other means (i.e., volcanism; see Figure S4 for size estimation with different percentage of impact contribution to the Os_i shift) or even larger if the input of radiogenic Os from weathering has diminished the unradiogenic Os signal. For a 3.3 km diameter comet, the Os content is estimated to be 6.32×10^{18} ng, which is about 7.9% of the K-Pg impactor (8×10^{19} ng Os; Paquay et al., 2008). The Ir content is estimated to be 5.93×10^{18} ng. This amount equals a global Ir flux of 1.16 ng/cm^2 , which is just 2% of that calculated for the Cretaceous-Paleogene boundary (55 ng/cm^2 ; Paquay et al., 2008) and 13% of the Late Eocene impactor (9 ng/cm^2 ; Paquay et al., 2008). The low flux could explain why only small Ir spikes are found in other P-E sections (Dolenec et al., 2000; Schmitz et al., 1997), and none observed in the records studied here.

Additional impactor-driven Earth system effects include formation and upper atmosphere disbursement of sulfate aerosols, which are known to cause short-lived climate cooling when emitted by other sources such as explosive volcanic eruptions (Kring et al., 1996). We estimate that a 3.3 km diameter comet would contain ~ 0.76 Gt of sulfur (see supporting information S1), $\sim 3,000$ times the current atmospheric sulfur mass (Kring et al., 1996). To assess the climatic impact of cometary magnitude stratospheric sulfate, we use the WACCM chemistry-climate model (Marsh et al., 2013) coupled with the Community Aerosol and Radiation Model for Atmospheres (Bardeen et al., 2008) to simulate both a baseline climate and that perturbed by an impactor. In

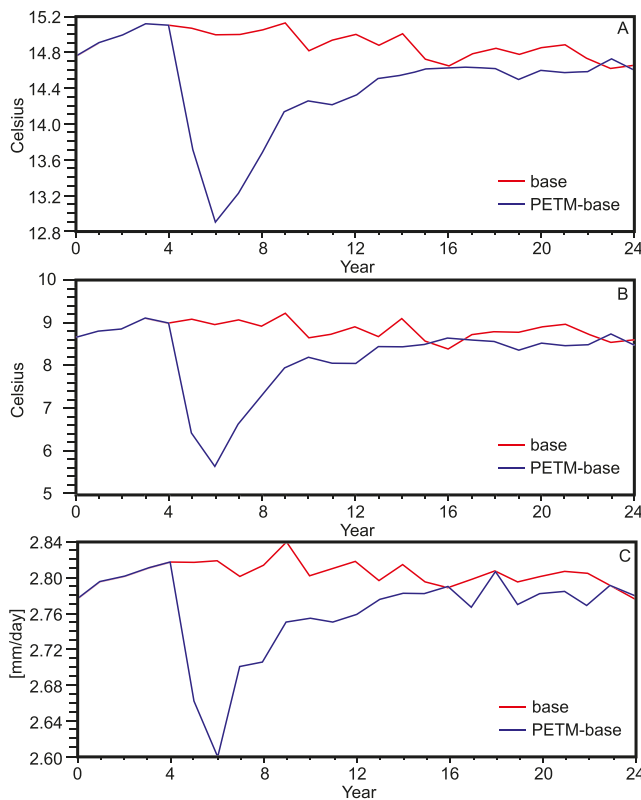


Figure 3. WACCM-CARMA simulated effects of impact aerosols on mean annual sea surface temperature (a), mean annual land temperature (b), and mean annual global precipitation (c). Impact aerosols were introduced in Year 5.

amount needed ($\geq 3,000\text{--}10,000$ Gt) to drive the PETM (Cui et al., 2011; Gutjahr et al., 2017; Zeebe et al., 2009). Thus, a comet alone cannot account for the carbon influx needed to drive the CIE and associated climate change of the PETM. As such, other sources of isotopically light carbon are needed to drive the PETM. However, it should be noted that the 0.4 Gt carbon from the comet would have been brought into the Earth system instantly and escalated $p\text{CO}_2$ rapidly, which may have increased the importance of that input, depending on the duration of PETM onset and the exact rate of terrestrial carbon emissions that contributed to it. The comet might have enhanced its warming effect if the target lithology was hydrocarbon-rich sediments, which would have increased the quantity of carbon released into the atmosphere by the impact. It has also been speculated that an impactor may have triggered the release of other carbon reservoirs such

our impactor simulation, we assume land-based impact and full conversion of sulfur to SO_2 (Fung et al., 2019), that is, we instantaneously add 1.52 Gt of SO_2 to the stratosphere (50 km), 2 orders of magnitude greater than recent annual global volcanic SO_2 emissions [0.023 Gt/year; Carn et al., 2017], and more than half of estimated Deccan Trap annual emissions (2.4 Gt/year; Schmidt et al., 2016). Since the SO_2 is injected in the upper atmosphere and its effects are primarily assessed at the global rather than local scale, our WACCM simulations use modern boundary conditions rather than Late Paleocene, an assumption that is unlikely to affect the large-scale atmospheric circulation (Tabor et al., 2016). Simulations indicate global cooling of the oceans and land within 2 years of the impact (Figure 3; global average sea surface temperature falls by ~ 2.2 °C; land average temperature falls by ~ 3.5 °C; Figures 3a, 3b, and 4). SO_2 emissions from NAIP lava flows might also have caused climate cooling immediately prior to/during the PETM; thus, a combined effect of both the volcanism and impact could have prolonged and worsened the climate cooling. Temperatures require more than a decade to recover to preimpact values. Cooling also leads to a 7% decrease in global precipitation shortly after the impact (Figures 3c and 4). To date, no depositional evidence for episodic cooling and/or reduced precipitation has been recovered; however, settings with higher temporal resolution may record these environmental changes and should be investigated. Despite short-term cooling, it is unlikely that the comet impact would have appreciably influenced the overall PETM warming trend.

Although our data suggest that both large-scale volcanism and a comet impact are associated with the P-E interval, it remains unclear to what extent they contributed to the carbon influx required to drive the PETM hyperthermal. Our geochemistry model estimates the cometary carbon to be ~ 0.4 Gt (see supporting information S1), which is far less than the

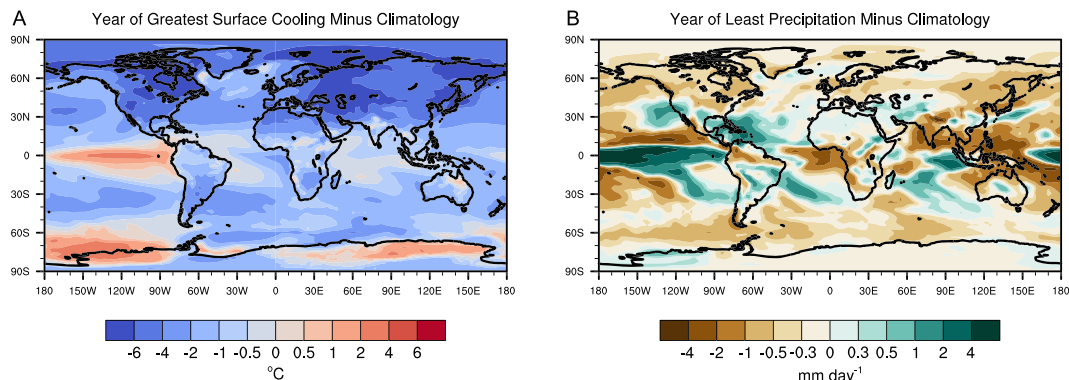


Figure 4. WACCM-CARMA simulations of surface temperature (A) and precipitation (B) perturbations due to the introduction of stratospheric sulfate aerosols commensurate with an ~ 3.3 km comet impact.

as destabilization of gas hydrates, causing further rapid injection of greenhouse gas into the environment (Cramer & Kent, 2005).

5. Conclusion

Our study suggests that both a comet (~3.3 km diameter) impact event and volcanism are associated with climate perturbations during the P-E interval. Carbon from the comet alone cannot account for the full manifestation of the CIE. However, the comet impact may have caused transient global cooling and reduced precipitation just prior to the better-known P-E climate warming. Comet impact, large-scale volcanism, and other sources of carbon (dissolution of methane hydrates and thermogenic volatiles, etc.) might have jointly caused the environmental disruption at the P-E boundary.

Acknowledgments

Samples were provided by IODP, which is sponsored by NSF and participating countries under management of the Joint Oceanographic Institutions, Inc. We gratefully acknowledge the TOTAL Endowment Fund and the CUG Wuhan Dida Scholarship to D. S. and the University of Durham and China Scholarship Council to Z. L. We acknowledge the support of Antonia Hoffman, Geoff Nowell, and Chris Ottley. D. E. H. thanks the QUEST high performance computing facility at Northwestern University for computational, storage, and staff resources. C. R. T. thanks Charles Bardeen for assistance setting up the model configuration. L. M. E. P. thanks the University of Lausanne for the use of their Hg facilities and financial support. Data available from Mendeley Data (<https://doi.org/10.17632/zyw7cyw88r.1>).

References

- Bardeen, C. G., Toon, O. B., Jensen, E. J., Marsh, D. R., & Harvey, V. L. (2008). Numerical simulations of the three-dimensional distribution of meteoric dust in the mesosphere and upper stratosphere. *Journal of Geophysical Research*, 113, D17202. <https://doi.org/10.1029/2007JD009515>
- Bowen, G. J., Maibauer, B. J., Kraus, M. J., Rohl, U., Westerhold, T., Steinke, A., et al. (2015). Two massive, rapid releases of carbon during the onset of the Palaeocene–Eocene thermal maximum. *Nature Geoscience*, 8(1), 44–47. <https://doi.org/10.1038/ngeo2316>, <http://www.nature.com/ngeo/journal/v8/n1/abs/ngeo2316.html#supplementary-information>
- Canfield, D. E., Raiswell, R., Westrich, J. T., Reaves, C. M., & Berner, R. A. (1986). The use of chromium reduction in the analysis of reduced inorganic sulfur in sediments and shales. *Chemical Geology*, 54(1), 149–155. [https://doi.org/10.1016/0009-2541\(86\)90078-1](https://doi.org/10.1016/0009-2541(86)90078-1)
- Carn, S. A., Fioletov, V. E., McLinden, C. A., Li, C., & Krotkov, N. A. (2017). A decade of global volcanic SO₂ emissions measured from space. *Scientific Reports*, 7, 44095. <https://doi.org/10.1038/srep44095>, <https://www.nature.com/articles/srep44095.html#supplementary-information>
- Chu, Z., Yan, Y., Chen, Z., Guo, J., Yang, Y., Li, C., & Zhang, Y. (2015). A comprehensive method for precise determination of Re, Os, Ir, Ru, Pt, Pd concentrations and Os isotopic compositions in geological samples. *Geostandards and Geoanalytical Research*, 39(2), 151–169. <https://doi.org/10.1111/j.1751-908X.2014.00283.x>
- Cramer, B. S., & Kent, D. V. (2005). Bolide summer: The Paleocene–Eocene Thermal Maximum as a response to an extraterrestrial trigger. *Palaeogeography, Palaeoclimatology, Palaeoecology*, 224(1–3), 144–166. <https://doi.org/10.1016/j.palaeo.2005.03.040>
- Creaser, R. A., Papanastassiou, D. A., & Wasserburg, G. J. (1991). Negative thermal ion mass spectrometry of osmium, rhenium and iridium. *Geochimica et Cosmochimica Acta*, 55(1), 397–401. [https://doi.org/10.1016/0016-7037\(91\)90427-7](https://doi.org/10.1016/0016-7037(91)90427-7)
- Cui, Y., Kump, L. R., Ridgwell, A. J., Charles, A. J., Junium, C. K., Diefendorf, A. F., et al. (2011). Slow release of fossil carbon during the Palaeocene–Eocene Thermal Maximum. *Nature Geoscience*, 4, 481. <https://doi.org/10.1038/ngeo1179>, <https://www.nature.com/articles/ngeo1179.html#supplementary-information>
- Dickens, G. R., O’Neil, J. R., Rea, D. K., & Owen, R. M. (1995). Dissociation of oceanic methane hydrate as a cause of the carbon isotope excursion at the end of the Paleocene. *Paleoceanography*, 10(6), 965–971. <https://doi.org/10.1029/95pa02087>
- Dickson, A. J., Cohen, A. S., Coe, A. L., Davies, M., Shcherbinina, E. A., & Gavrilov, Y. O. (2015). Evidence for weathering and volcanism during the PETM from Arctic Ocean and Peri-Tethys osmium isotope records. *Palaeogeography, Palaeoclimatology, Palaeoecology*, 438, 300–307. <https://doi.org/10.1016/j.palaeo.2015.08.019>
- Dolenec, T., Pavšič, J., & Lojen, S. (2000). Ir anomalies and other elemental markers near the Palaeocene–Eocene boundary in a flysch sequence from the Western Tethys (Slovenia). *Terra Nova*, 12(5), 199–204. <https://doi.org/10.1046/j.1365-3121.2000.00292.x>
- Engleman, E. E., Jackson, L. L., & Norton, D. R. (1985). Determination of carbonate carbon in geological materials by coulometric titration. *Chemical Geology*, 53(1), 125–128. [https://doi.org/10.1016/0009-2541\(85\)90025-7](https://doi.org/10.1016/0009-2541(85)90025-7)
- Fung, M. K., Schaller, M. F., Hoff, C. M., Katz, M. E., & Wright, J. D. (2019). Widespread and intense wildfires at the Paleocene–Eocene boundary. *Geochemical Perspectives Letters*, 10, 1–6. <https://doi.org/10.7185/geochemlett.1906>
- Gingerich, P. D. (2003). Mammalian responses to climate change at the Paleocene–Eocene boundary: Polecat Bench record in the northern Bighorn Basin, Wyoming. In S. L. Wing, P. D. Gingerich, B. Schmitz, & E. Thomas (Eds.), *Causes and consequences of globally warm climates in the early Paleogene*, GSA Special Paper 369 (Vol. 369, pp. 463–478). Boulder, Colorado: Geological Society of America. <https://doi.org/10.1130/0-8137-2369-8.463>
- Goderis, S., Tagle, R., Belza, J., Smit, J., Montanari, A., Vanhaecke, F., et al. (2013). Reevaluation of siderophile element abundances and ratios across the Cretaceous–Paleogene (K–Pg) boundary: Implications for the nature of the projectile. *Geochimica et Cosmochimica Acta*, 120, 417–446. <https://doi.org/10.1016/j.gca.2013.06.010>
- Gutjahr, M., Ridgwell, A., Sexton, P. F., Anagnostou, E., Pearson, P. N., Pälike, H., et al. (2017). Very large release of mostly volcanic carbon during the Palaeocene–Eocene Thermal Maximum. *Nature*, 548(7669), 573–577. <https://doi.org/10.1038/nature23646>, <https://www.nature.com/articles/nature23646.html#supplementary-information>
- Higgins, J. A., & Schrag, D. P. (2006). Beyond methane: Towards a theory for the Paleocene–Eocene Thermal Maximum. *Earth and Planetary Science Letters*, 245(3–4), 523–537. <https://doi.org/10.1016/j.epsl.2006.03.009>
- Huffman, E. W. D. (1977). Performance of a new automatic carbon dioxide coulometer. *Microchemical Journal*, 22(4), 567–573. [https://doi.org/10.1016/0026-265X\(77\)90128-X](https://doi.org/10.1016/0026-265X(77)90128-X)
- Jansa, L. F. (1993). Cometary impacts into ocean: Their recognition and the threshold constraint for biological extinctions. *Palaeogeography, Palaeoclimatology, Palaeoecology*, 104(1), 271–286. [https://doi.org/10.1016/0031-0182\(93\)90137-8](https://doi.org/10.1016/0031-0182(93)90137-8)
- Jones, M. T., Percival, L. M. E., Stokke, E. W., Frieling, J., Mather, T. A., Riber, L., et al. (2019). Mercury anomalies across the Palaeocene–Eocene Thermal Maximum. *Climate of the Past*, 15(1), 217–236. <https://doi.org/10.5194/cp-15-217-2019>
- Katz, M. E., Pak, D. K., Dickens, G. R., & Miller, K. G. (1999). The source and fate of massive carbon input during the latest Paleocene Thermal Maximum. *Science*, 286(5444), 1531–1533. <https://doi.org/10.1126/science.286.5444.1531>

- Keller, G., Mateo, P., Punekar, J., Khozyem, H., Gertsch, B., Spangenberg, J., et al. (2018). Environmental changes during the Cretaceous-Paleogene mass extinction and Paleocene-Eocene Thermal Maximum: Implications for the Anthropocene. *Gondwana Research*, 56, 69–89. <https://doi.org/10.1016/j.gr.2017.12.002>
- Kring, D. A., Melosh, H. J., & Hunten, D. M. (1996). Impact-induced perturbations of atmospheric sulfur. *Earth and Planetary Science Letters*, 140(1), 201–212. [https://doi.org/10.1016/0012-821X\(96\)00050-7](https://doi.org/10.1016/0012-821X(96)00050-7)
- Marsh, D. R., Mills, M. J., Kinnison, D. E., Lamarque, J.-F., Calvo, N., & Polvani, L. M. (2013). Climate change from 1850 to 2005 simulated in CESM1(WACCM). *Journal of Climate*, 26(19), 7372–7391. <https://doi.org/10.1175/JCLI-D-12-00558.1>
- Paquay, F. S., Ravizza, G. E., Dalai, T. K., & Peucker-Ehrenbrink, B. (2008). Determining chondritic impactor size from the marine osmium isotope record. *Science*, 320(5873), 214–218. <https://doi.org/10.1126/science.1152860>
- Percival, L. M. E., Jenkyns, H. C., Mather, T. A., Dickson, A. J., Batenburg, S. J., Ruhl, M., et al. (2018). Does large igneous province volcanism always perturb the mercury cycle? Comparing the records of Oceanic Anoxic Event 2 and the end-Cretaceous to other Mesozoic events. *American Journal of Science*, 318(8), 799–860. <https://doi.org/10.2475/08.2018.01>
- Percival, L. M. E., Ruhl, M., Hesselbo, S. P., Jenkyns, H. C., Mather, T. A., & Whiteside, J. H. (2017). Mercury evidence for pulsed volcanism during the end-Triassic mass extinction. *Proceedings of the National Academy of Sciences*, 114(30), 7929–7934. <https://doi.org/10.1073/pnas.1705378114>
- Peucker-Ehrenbrink, B., & Ravizza, G. (2000). The marine osmium isotope record. *Terra Nova*, 12(5), 205–219. <https://doi.org/10.1046/j.1365-3212.2000.00295.x>
- Ravizza, G., Norris, R. N., Blusztajn, J., & Aubrey, M. P. (2001). An osmium isotope excursion associated with the late Paleocene Thermal Maximum: Evidence of intensified chemical weathering. *Paleoceanography*, 16(2), 155–163. <https://doi.org/10.1029/2000PA000541>
- Saunders, A. D. (2016). Two LIPs and two Earth-system crises: The impact of the North Atlantic Igneous Province and the Siberian Traps on the Earth-surface carbon cycle. *Geological Magazine*, 153(2), 201–222. <https://doi.org/10.1017/S0016756815000175>
- Schaller, M. F., Fung, M. K., Wright, J. D., Katz, M. E., & Kent, D. V. (2016). Impact ejecta at the Paleocene-Eocene boundary. *Science*, 354(6309), 225–229. <https://doi.org/10.1126/science.aaf5466>
- Schaller, M. F., Turrin, B. D., Fung, M. K., Katz, M. E., & Swisher, C. C. (2019). Initial 40Ar-39Ar ages of the Paleocene-Eocene boundary impact spherules. *Geophysical Research Letters*, 46, 9091–9102. <https://doi.org/10.1029/2019GL082473>
- Schmidt, A., Skeffington, R. A., Thordarson, T., Self, S., Forster, P. M., Rap, A., et al. (2016). Selective environmental stress from sulphur emitted by continental flood basalt eruptions. *Nature Geoscience*, 9(1), 77–84. <https://doi.org/10.1038/NGEO2588>
- Schmitz, B., Asaro, F., Molina, E., Monechi, S., von Salis, K., & Speijer, R. P. (1997). High-resolution iridium, $\delta^{13}\text{C}$, $\delta^{18}\text{O}$, foraminifera and nannofossil profiles across the latest Paleocene benthic extinction event at Zumaya, Spain. *Palaeogeography, Palaeoclimatology, Palaeoecology*, 133(1), 49–68. [https://doi.org/10.1016/S0031-0182\(97\)00024-2](https://doi.org/10.1016/S0031-0182(97)00024-2)
- Schmitz, B., Peucker-Ehrenbrink, B., Heilmann-Clausen, C., Åberg, G., Asaro, F., & Lee, C.-T. A. (2004). Basaltic explosive volcanism, but no comet impact, at the Paleocene-Eocene boundary: High-resolution chemical and isotopic records from Egypt, Spain and Denmark. *Earth and Planetary Science Letters*, 225(1-2), 1–17. <https://doi.org/10.1016/j.epsl.2004.06.017>
- Schmitz, B., & Pujalte, V. (2003). Sea-level, humidity, and land-erosion records across the initial Eocene thermal maximum from a continental-marine transect in northern Spain. *Geology*, 31(8), 689–692. <https://doi.org/10.1130/g19527.1>
- Selby, D., & Creaser, R. A. (2003). Re-Os geochronology of organic rich sediments: An evaluation of organic matter analysis methods. *Chemical Geology*, 200(3-4), 225–240. [https://doi.org/10.1016/S0009-2541\(03\)00199-2](https://doi.org/10.1016/S0009-2541(03)00199-2)
- Selby, D., Creaser, R. A., & Fowler, M. G. (2007). Re-Os elemental and isotopic systematics in crude oils. *Geochimica et Cosmochimica Acta*, 71(2), 378–386. <https://doi.org/10.1016/j.gca.2006.09.005>
- Shen, J., Algeo, T. J., Chen, J., Planavsky, N. J., Feng, Q., Yu, J., & Liu, J. (2019). Mercury in marine Ordovician/Silurian boundary sections of South China is sulfide-hosted and non-volcanic in origin. *Earth and Planetary Science Letters*, 511, 130–140. <https://doi.org/10.1016/j.epsl.2019.01.028>
- Sholupov, S. E., & Ganeyev, A. A. (1995). Zeeman atomic absorption spectrometry using high frequency modulated light polarization. *Spectrochimica Acta Part B: Atomic Spectroscopy*, 50(10), 1227–1236. [https://doi.org/10.1016/0584-8547\(95\)01316-7](https://doi.org/10.1016/0584-8547(95)01316-7)
- Svensen, H., Planke, S., Malthe-Sørensen, A., Jamtveit, B., Myklebust, R., Rasmussen Eidem, T., & Rey, S. S. (2004). Release of methane from a volcanic basin as a mechanism for initial Eocene global warming. *Nature*, 429(6991), 542–545. <https://doi.org/10.1038/nature02566>
- Tabor, C. R., Poulsen, C. J., Lunt, D. J., Otto-Bliesner, B. L., Rosenbloom, N., Brady, E. C., et al. (2016). The cause of Late Cretaceous cooling: A multimodel-proxy comparison. *Geology*, 44(11), 963–966. <https://doi.org/10.1130/G38363.1>
- Walker, J. C. G., Hays, P. B., & Kasting, J. F. (1981). A negative feedback mechanism for the long-term stabilization of Earth's surface temperature. *Journal of Geophysical Research*, 86(C10), 9776–9782. <https://doi.org/10.1029/JC086iC10p09776>
- Wasson, J. T., & Kallemeyn, G. W. (1988). Compositions of chondrites. *Philosophical Transactions of the Royal Society of London. Series A, Mathematical and Physical Sciences*, 325(1587), 535. <https://doi.org/10.1098/rsta.1988.0066>
- Wieczorek, R., Fantle, M. S., Kump, L. R., & Ravizza, G. (2013). Geochemical evidence for volcanic activity prior to and enhanced terrestrial weathering during the Paleocene Eocene Thermal Maximum. *Geochimica et Cosmochimica Acta*, 119, 391–410. <https://doi.org/10.1016/j.gca.2013.06.005>
- Wing, S. L., Harrington, G. J., Smith, F. A., Bloch, J. I., Boyer, D. M., & Freeman, K. H. (2005). Transient floral change and rapid global warming at the Paleocene-Eocene Boundary. *Science*, 310(5750), 993–996. <https://doi.org/10.1126/science.1116913>
- Wright, J. D., & Schaller, M. F. (2013). Evidence for a rapid release of carbon at the Paleocene-Eocene thermal maximum. *Proceedings of the National Academy of Sciences*, 110(40), 15908–15913. <https://doi.org/10.1073/pnas.1309188110>
- Zachos, J., Pagani, M., Sloan, L., Thomas, E., & Billups, K. (2001). Trends, rhythms, and aberrations in global climate 65 Ma to present. *Science*, 292(5517), 686–693. <https://doi.org/10.1126/science.1059412>
- Zeebe, R. E., Zachos, J. C., & Dickens, G. R. (2009). Carbon dioxide forcing alone insufficient to explain Palaeocene-Eocene Thermal Maximum warming. *Nature Geoscience*, 2, 576. <https://doi.org/10.1038/ngeo578>, <https://www.nature.com/articles/ngeo578#supplementary-information>

References From the Supporting Information

- Bardeen, C. G., Garcia, R. R., Toon, O. B., & Conley, A. J. (2017). On transient climate change at the Cretaceous–Paleogene boundary due to atmospheric soot injections. *Proceedings of the National Academy of Sciences*, 114(36), E7415–E7424. <https://doi.org/10.1073/pnas.1708980114>

- Cochran, A. L., Levasseur-Regourd, A. C., Cordiner, M., Hadamcik, E., Lasue, J., Gicquel, A., et al. (2015). The composition of comets. *Space Science Reviews*, 197(1-4), 9–46. <https://doi.org/10.1007/s11214-015-0183-6>
- Danabasoglu, G., Bates, S. C., Briegleb, B. P., Jayne, S. R., Jochum, M., Large, W. G., et al. (2011). The CCSM4 Ocean Component. *Journal of Climate*, 25(5), 1361–1389. <https://doi.org/10.1175/JCLI-D-11-0091.1>
- Gent, P. R., Danabasoglu, G., Donner, L. J., Holland, M. M., Hunke, E. C., Jayne, S. R., et al. (2011). The Community Climate System Model Version 4. *Journal of Climate*, 24(19), 4973–4991. <https://doi.org/10.1175/2011JCLI4083.1>
- Hunke, E. C., & Lipscomb, W. H. (2008). CICE: The Los Alamos sea ice model, documentation and software user's manual, 87545.
- Hurrell, J. W., Ghosh, S., Kay, J. E., Kushner, P. J., Lamarque, J.-F., Large, W. G., et al. (2013). The Community Earth System Model: A framework for collaborative research. *BAMS*, 94(9), 1339–1360. <https://doi.org/10.1175/bams-d-12-00121.1>
- Lawrence, D. M., Oleson, K. W., Flanner, M. G., Fletcher, C. G., Lawrence, P. J., Levis, S., et al. (2011). The CCSM4 Land Simulation, 1850–2005: Assessment of surface climate and new capabilities. *Journal of Climate*, 25(7), 2240–2260. <https://doi.org/10.1175/JCLI-D-11-00103.1>
- Toon, O. B., Bardeen, C., & Garcia, R. (2016). Designing global climate and atmospheric chemistry simulations for 1 and 10 km diameter asteroid impacts using the properties of ejecta from the K-Pg impact. *Atmospheric Chemistry and Physics*, 16(20), 13185–13212. <https://doi.org/10.5194/acp-16-13185-2016>
- Toon, O. B., Turco, R. P., Westphal, D., Malone, R., & Liu, M. (1988). A multidimensional model for aerosols: Description of computational analogs. *Journal of the Atmospheric Sciences*, 45(15), 2123–2144. [https://doi.org/10.1175/1520-0469\(1988\)045<2123:AMMFAD>2.0.CO;2](https://doi.org/10.1175/1520-0469(1988)045<2123:AMMFAD>2.0.CO;2)
- Wooden, D. H., Ishii, H. A., & Zolensky, M. E. (2017). Cometary dust: The diversity of primitive refractory grains. *Philosophical Transactions. Series A, Mathematical, Physical, and Engineering Sciences*, 375(2097), 20160260. <https://doi.org/10.1098/rsta.2016.0260>